

2

3 **Fluor-elbaite, Na(Li_{1.5}Al_{1.5})Al₆(Si₆O₁₈)(BO₃)₃(OH)₃F, a new mineral species of**
4 **the tourmaline supergroup**

5 FERDINANDO BOSI¹, GIOVANNI B. ANDREOZZI¹, HENRIK SKOGBY², AARON J. LUSSIER³, YASSIR
6 ABDU³ AND FRANK C. HAWTHORNE³

7

8 ¹Dipartimento di Scienze della Terra, Sapienza Università di Roma, P.le A. Moro, 5, I-00185 Rome, Italy

9 ²Department of Mineralogy, Swedish Museum of Natural History, Box 50007, SE-10405 Stockholm, Sweden

10 ³Department of Geological Sciences, University of Manitoba, Winnipeg, Manitoba R3T 2N2, Canada
11

12

13

14 **ABSTRACT**

15

16 Fluor-elbaite, Na(Li_{1.5}Al_{1.5})Al₆(Si₆O₁₈)(BO₃)₃(OH)₃F, is a new mineral of the tourmaline
17 supergroup. It is found in miarolitic cavities in association with quartz, pink muscovite,
18 lepidolite, spodumene, spessartine and pink beryl in the Cruzeiro and Urubu mines (Minas
19 Gerais, Brazil), and apparently formed from late-stage hydrothermal solutions related to the
20 granitic pegmatite. Crystals are blue-green with a vitreous luster, sub-conchoidal fracture and
21 white streak. Fluor-elbaite has a Mohs hardness of approximately 7.5, and has a calculated
22 density of about 3.1 g/cm³. In plane-polarized light, fluor-elbaite is pleochroic (O = green/bluish
23 green, E = pale green), uniaxial negative. Fluor-elbaite is rhombohedral, space group *R3m*, *a* =
24 15.8933(2), *c* = 7.1222(1) Å, *V* = 1558.02(4) Å³, *Z* = 3 (for the Cruzeiro material). The strongest
25 eight X-ray-diffraction lines in the powder pattern [*d* in Å(*I*)(*hkl*)] are: 2.568(100)(051),
26 2.939(92)(122), 3.447(67)(012), 3.974(58)(220), 2.031(57)(152), 4.200(49)(211), 1.444(32)(642)
27 and 1.650(31)(063). Analysis by a combination of electron microprobe, secondary ion mass
28 spectrometry and Mössbauer spectroscopy gives SiO₂ = 37.48, Al₂O₃ = 37.81, FeO = 3.39, MnO
29 = 2.09, ZnO = 0.27, CaO = 0.34, Na₂O = 2.51, K₂O = 0.06, F = 1.49, B₂O₃ = 10.83, Li₂O = 1.58,

30 $\text{H}_2\text{O} = 3.03$, sum 100.25 wt%. The unit formula is: $^{\text{X}}(\text{Na}_{0.78}\square_{0.15}\text{Ca}_{0.06}\text{K}_{0.01})$
31 $^{\text{Y}}(\text{Al}_{1.15}\text{Li}_{1.02}\text{Fe}^{2+}_{0.46}\text{Mn}^{2+}_{0.28}\text{Zn}_{0.03})^{\text{Z}}\text{Al}_6^{\text{T}}(\text{Si}_{6.02}\text{O}_{18})^{\text{B}}(\text{BO}_3)_3^{\text{V}}(\text{OH})_3^{\text{W}}(\text{F}_{0.76}\text{OH}_{0.24})$.

32 The crystal structure of fluor-elbaite was refined to statistical indices $R1$ for all reflections
33 less than 2% using $\text{MoK}\alpha$ X-ray intensity data. Fluor-elbaite shows relations with elbaite and
34 tsilaisite through the substitutions $^{\text{W}}\text{F} \leftrightarrow ^{\text{W}}\text{OH}$ and $^{\text{Y}}(\text{Al} + \text{Li}) + ^{\text{W}}\text{F} \leftrightarrow 2^{\text{Y}}\text{Mn}^{2+} + ^{\text{W}}\text{OH}$,
35 respectively.

36

37

INTRODUCTION

38

39 The tourmaline supergroup minerals occur typically as accessory phases (but occasionally
40 as minor or even major minerals) in a wide range of rocks of different origin and composition,
41 including granitic pegmatites. They are well-known as valuable indicator minerals that can
42 provide information on the compositional evolution of their host rocks, chiefly due to their
43 ability to incorporate a large number of elements (e.g., Novák et al. 2004; Agrosi et al. 2006;
44 Lussier et al. 2011a; Novák et al. 2011; Van Hinsberg et al. 2011). However, the chemical
45 composition of tourmalines is also strongly controlled by various crystal-structural constraints
46 (e.g., Hawthorne 1996, 2002; Bosi 2010, 2011; Henry and Dutrow 2011) as well as by
47 temperature (van Hinsberg and Schumacher 2011).

48 The crystal structure and crystal chemistry of tourmaline have been extensively studied
49 (e.g., Foit 1989; Hawthorne 1996; Hawthorne and Henry 1999; Bosi and Lucchesi 2007; Lussier
50 et al. 2008; Bosi et al. 2010; Lussier et al. 2011a, b). The general formula of tourmaline may be
51 written as: $\text{XY}_3\text{Z}_6\text{T}_6\text{O}_{18}(\text{BO}_3)_3\text{V}_3\text{W}$, where $\text{X} (\equiv [^9]\text{X}) = \text{Na}^+, \text{K}^+, \text{Ca}^{2+}, \square$ (=vacancy); $\text{Y} (\equiv [^6]\text{Y})$
52 $= \text{Al}^{3+}, \text{Fe}^{3+}, \text{Cr}^{3+}, \text{V}^{3+}, \text{Mg}^{2+}, \text{Fe}^{2+}, \text{Mn}^{2+}, \text{Li}^+$; $\text{Z} (\equiv [^6]\text{Z}) = \text{Al}^{3+}, \text{Fe}^{3+}, \text{Cr}^{3+}, \text{V}^{3+}, \text{Mg}^{2+}, \text{Fe}^{2+}$; $\text{T} (\equiv$
53 $[^4]\text{T}) = \text{Si}^{4+}, \text{Al}^{3+}, \text{B}^{3+}$; $\text{B} (\equiv [^3]\text{B}) = \text{B}^{3+}$; $\text{W} (\equiv [^3]\text{O1}) = \text{OH}^{1-}, \text{F}^{1-}, \text{O}^{2-}$; $\text{V} (\equiv [^3]\text{O3}) = \text{OH}^{1-}, \text{O}^{2-}$ and
54 where, for example, T represents a group of cations ($\text{Si}^{4+}, \text{Al}^{3+}, \text{B}^{3+}$) accommodated at the [4]-
55 coordinated T sites. The dominance of such ions at one or more sites of the structure gives rise to
56 many distinct mineral species (Henry et al. 2011).

57 A previous study on the crystal chemistry of the tourmaline-supergroup minerals
58 (Federico et al. 1998) demonstrated the presence of the “fluor-“ equivalent of elbaite in the
59 Cruzeiro mine (Minas Gerais, Brazil). Moreover, the fluor-elbaite end-member was predicted by
60 Hawthorne and Henry (1999) with the ideal formula $\text{Na}(\text{Li}_{1.5}\text{Al}_{1.5})\text{Al}_6\text{Si}_6\text{O}_{18}(\text{BO}_3)_3(\text{OH})_3\text{F}$,

61 derived from the root composition of elbaite, $\text{Na}(\text{Li}_{1.5}\text{Al}_{1.5})\text{Al}_6(\text{Si}_6\text{O}_{18})(\text{BO}_3)_3(\text{OH})_3\text{OH}$, via the
62 substitution $\text{F} \rightarrow \text{OH}$ at the W position.

63 A formal description of the new species fluor-elbaite is presented here, including a full
64 characterization of its physical, chemical and structural attributes. The name has been assigned
65 according to the chemical composition, as recommended by Henry et al. (2011). The new species
66 as well as the new name have been approved by the Commission on New Minerals,
67 Nomenclature and Classification of the International Mineralogical Association (IMA 2011-
68 071). The holotype specimen from the Cruzeiro mine is deposited in the collections of the
69 Museum of Mineralogy, Earth Sciences Department, Sapienza University of Rome, Italy,
70 catalogue number 33045. The holotype specimen from the Urubu mine is deposited in the
71 collection of the Department of Natural History, Royal Ontario Museum, 100. Queens Park,
72 Toronto, Ontario M5S 2C6, Canada, catalogue number M56418.

73

74

75 OCCURRENCE, APPEARANCE, PHYSICAL AND OPTICAL PROPERTIES

76

77 The fluor-elbaite specimens here examined occur at two deposits. The first one is the
78 Cruzeiro mine (São José da Safira, Minas Gerais, Brazil), where tourmaline is associated with
79 quartz, pink muscovite, lepidolite, spodumene, spessartine and pink beryl (Federico et al. 1998).
80 The mineral is also found in the Urubu mine (Itinga, Minas Gerais, Brazil), but in this case
81 associated minerals are not known. Both the Cruzeiro and Urubu fluor-elbaite crystals formed
82 from late-stage hydrothermal solutions inside (or close to) miarolitic cavities of the granitic
83 pegmatite (e.g., Federico et al. 1998). The crystal from Cruzeiro is a euhedral, inclusion-free,
84 blue-green, elongated prism. It was cut in slices for analytical purposes. The remaining slice is
85 approximately $4 \times 4 \times 1$ mm in size (Fig. 1). The crystal from Urubu is a euhedral, blue-green,
86 elongated prism approximately $1.3 \times 1.2 \times 2.3$ cm in size.

87 The fluor-elbaite morphology consists of elongated $\{10\bar{1}0\}$ and $\{11\bar{2}0\}$ prisms with
88 striated faces terminated by a prominent $\{0001\}$ pedion (Fig. 2). The crystals are brittle with a
89 vitreous luster, sub-conchoidal fracture and white streak; Mohs hardness is approximately 7.5.
90 The calculated density is 3.091 g/cm^3 (Cruzeiro) and 3.123 g/cm^3 (Urubu). In transmitted light,
91 the investigated fluor-elbaite samples are pleochroic with O = green and E = pale green

92 (Cruzeiro) and O = bluish green and E = pale green (Urubu). Fluor-elbaite is uniaxial negative
93 with refractive indices of $\omega = 1.640(5)$, $\varepsilon = 1.625(5)$ measured by the immersion method using
94 white light from a tungsten source (Cruzeiro), and $\omega = 1.648(2)$, $\varepsilon = 1.629(2)$ measured with gel-
95 filtered Na light ($\lambda = 589.9$ nm) (Urubu). The mean index of refraction, density and chemical
96 composition lead to excellent (Cruzeiro) and superior (Urubu) compatibility indices ($1 - K_p/K_c =$
97 0.026 and 0.018 , respectively) (Mandarino 1976, 1981).

98 It is worth pointing out that the blue-green bulk color as well as the pleochroism observed
99 for the present crystals is most likely caused by minor concentrations of chromophores (e.g., Fe
100 and Mn). Presumably, end-member fluor-elbaite will be colorless.

101

102

METHODS

103

104 Microprobe analysis

105 **Cruzeiro.** Chemical data for the fluor-elbaite from Cruzeiro were reported by Federico et
106 al. (1998) when describing sample 95V. In detail, 10 chemical spot analyses were done using an
107 electron microprobe in WDS mode (15 kV, 15 nA, 5 μm beam diameter). The light elements H,
108 Li and B were analyzed by an ion microprobe (secondary ion mass spectrometry, primary current
109 of oxygen negative, with an intensity of 5 nA, focused on 10 μm , secondary current of positive
110 ions, voltage offset of -60 V energy window of 10 V) after calibration against TG and AAS data
111 for H and Li, respectively, as well as against glasses and tourmaline samples for B (Federico et
112 al. 1998). However, the measured H_2O content was relatively high (3.34 ± 0.16 wt%), and would
113 give an anomalous excess of OH+F (4.31 ± 0.17 apfu) in the tourmaline formula. Consequently,
114 H_2O content was calculated by stoichiometry (3.03 apfu, Table 1). Note that the difference
115 between the measured and calculated H_2O values is within the analytical error (2σ).

116 **Urubu.** Chemical data for fluor-elbaite from Urubu were obtained primarily using a
117 Cameca SX100 electron microprobe (10 chemical spot analyses in WDS mode, 15 kV, 10 nA, 10
118 μm beam diameter). Li_2O and B_2O_3 were calculated from the stoichiometry. Hydrogen was
119 analyzed using a Cameca 7f SIMS. The relative ion signal of H^+ was normalized to Si^+ whose
120 concentration was measured by electron probe. Hydrogen and ^{28}Si were measured using a ~ 10 -
121 $15\mu\text{m}$ 6 nA primary beam of $^{16}\text{O}^-$ ions. The magnet was sequentially switched to collect
122 hydrogen and silicon. During analytical sessions, the sample accelerating voltage was set to +9.9

123 kV, with electrostatic analyzer in the secondary column set to accept +10 kV and an energy
124 window of ± 50 volts. This voltage offset was sufficient to suppress isobaric interferences during
125 analysis. The entrance slit was narrowed to obtain flat-top peaks at a mass resolving power of
126 about 400. Ions were detected with a Balzers SEV 1217 electron multiplier coupled with an ion-
127 counting system with an overall deadtime of 37 ns. The amount of H was quantified using elbaite
128 and cordierite of known chemical compositions Analytical data are summarized in Table 1.

129

130 **Mössbauer spectroscopy**

131 **Cruzeiro.** The oxidation state of Fe was determined by Mössbauer spectroscopy at room
132 temperature using a conventional spectrometer system operating in constant-acceleration mode.
133 In order to save sample material, the absorber was prepared by filling a small quantity of ground
134 material in a 1-mm hole in a lead plate, and the spectrum was acquired using a ^{57}Co point-source
135 in rhodium matrix with a nominal activity of 10 mCi. The spectrum was calibrated against α -Fe
136 foil and folded before fitting using the MDA software by Jernberg and Sundquist (1983). The
137 resultant spectrum (Fig. 3) shows an asymmetric doublet with hyperfine parameters typical for
138 Fe^{2+} , but no indications of Fe^{3+} . To account for the asymmetry, the spectrum was fitted with
139 three doublets assigned to Fe^{2+} ; however, these three doublets are not resolved and not
140 considered representing three distinctly different Fe^{2+} environments in the tourmaline structure.

141 **Urubu.** Mössbauer spectroscopy measurements were done in transmission geometry at
142 room temperature (RT) using a $^{57}\text{Co}(\text{Rh})$ point source. The spectrometer was calibrated with the
143 RT spectrum of α -Fe. In preparing the Mössbauer absorber, fluor-elbaite was mixed with sugar
144 and finely ground under acetone to avoid oxidation. The mixture was then loaded into a Pb ring
145 (2 mm inner diameter) and covered by tape on both sides. Assuming a recoilless fraction of 0.7
146 for the Mössbauer absorber, the amount of sample corresponds to an absorber thickness of ~ 4 mg
147 Fe/cm^2 . The spectra were analyzed using a Voigt-based quadrupole-splitting distribution (QSD)
148 method (Rancourt and Ping 1991). To account for absorber thickness effects, we allowed the
149 Lorentzian linewidth (Γ) of the symmetrical elemental doublets of the QSD to be an adjustable
150 parameter during the spectrum fitting (Rancourt 1994). However, full thickness correction was
151 applied to the Mössbauer data (Rancourt et al. 1993) and similar results ($\text{Fe}^{3+}/\text{Fe}^{2+}$) were
152 obtained from fitting of the thickness-corrected spectrum. The RT Mössbauer spectrum of the

153 Urubu fluor-elbaite (not shown) was also fitted by a model having three general sites for Fe²⁺
154 with no indication of Fe³⁺, in full agreement with that of the Cruzeiro sample.

155

156 **X-ray powder diffraction**

157 **Cruzeiro.** The X-ray powder-diffraction pattern for the sample from Cruzeiro was
158 collected using a Panalytical X'pert powder diffractometer equipped with an X'celerator silicon-
159 strip detector. The diffraction data (in Å for CuK, $\lambda = 1.54060$ Å), corrected using Si as an
160 internal standard, are listed in Table 2. Unit-cell parameters from the powder data were refined
161 using the program UnitCell (Holland and Redfern 1997): $a = 15.8970(6)$ Å, $c = 7.1227(3)$ Å, $V =$
162 $1558.9(1)$ Å³.

163 **Urubu.** X-ray powder-diffraction data for the sample from Urubu were collected with a
164 Bruker D8 Discover SuperSpeed micro-powder diffractometer with a multi-wire 2D detector
165 using a modified Gandolfi attachment, and indexed on $a = 15.915(3)$ Å, $c = 7.120(2)$ Å, $V =$
166 $1561.8(7)$ Å³. Data (in Å for CuK α) are listed in Table 2.

167

168 **Single-crystal structural refinement (SREF)**

169 **Cruzeiro.** A representative crystal of the type specimen was selected for X-ray
170 diffraction measurements on a Bruker KAPPA APEX-II single-crystal diffractometer (Sapienza
171 University of Rome, Earth Sciences Department), equipped with a CCD area detector (6.2×6.2
172 cm² active detection area, 512×512 pixels) and a graphite-crystal monochromator, using MoK α
173 radiation from a fine-focus sealed X-ray tube. The sample-to-detector distance was 4 cm. A total
174 of 4830 exposures (step = 0.2° , time/step = 20 s) covering a full reciprocal sphere with a
175 redundancy of about 10 were collected and a completeness of 99.7% was achieved. The
176 orientation of the crystal lattice was determined using more than 700 strong reflections, $I > 100$
177 $\sigma(I)$ evenly distributed in reciprocal space, and used for subsequent integration of all recorded
178 intensities. Final unit-cell parameters were refined by using the Bruker AXS SAINT program on
179 reflections with $I > 10 \sigma(I)$ in the range $6^\circ < 2\theta < 81^\circ$. The intensity data were processed and
180 corrected for Lorentz, polarization and background effects with the APEX2 software program of
181 Bruker AXS. The data were corrected for absorption using a multi-scan method (SADABS). The
182 absorption correction led to a significant improvement in R_{int} . No violations of $R3m$ symmetry
183 were noted.

184 Structure refinement was done with the SHELXL-97 program (Sheldrick 2008). Starting
185 coordinates were taken from Bosi et al. (2010). Variable parameters were: scale factor, extinction
186 coefficient, atomic coordinates, site scattering values expressed as mean atomic number (for X
187 and Y sites) and atomic displacement factors. To obtain the best values of statistical indexes ($R1$,
188 $wR2$), a fully ionized O scattering curve was used, whereas neutral scattering curves were used
189 for the other atoms. In detail, the X site was modeled using Na scattering factors. The occupancy
190 of the Y site was obtained considering the presence of Fe vs. Li. The Z, T, B and O1 sites were
191 modeled, respectively, with Al, Si, B and F scattering factors and with a fixed occupancy of 1,
192 because refinement with unconstrained occupancies showed no significant deviations from this
193 value. Following the findings of Burns et al. (1994) who reported high U_{eq} values for the O1 and
194 O2 sites that indicate position disorder, the crystal was refined twice, (1) with both sites
195 constrained to their positions of maximum site-symmetry, (00z) for O1 and (x, 1-x, z) for O2, and
196 (2) with both sites allowed to disorder with coordinates (x, x/2, z) and (x,y,z) (referred as split-site
197 SREF in this work). There were no correlations greater than 0.7 between the parameters at the
198 end of the refinement. Table 3 lists crystal data, data collection information and refinement
199 details; Table 4 gives the fractional atomic coordinates, equivalent isotropic displacement
200 parameters; Table 5 (on deposit) contains anisotropic displacement parameters; Table 6 shows
201 selected bond lengths.

202 **Urubu.** A single crystal was mounted on a Bruker D8 three-circle diffractometer
203 equipped with a rotating anode generator (MoK α X-radiation), multi-layer optics and an APEX-
204 II CCD detector. The intensities of 7994 reflections were collected to 60° 2 θ using 20s per 0.2°
205 frame with a crystal-to-detector distance of 5 cm. Empirical absorption corrections (SADABS;
206 Sheldrick 1996) were applied and identical data merged. Unit-cell parameters were obtained by
207 least-squares refinement of >1000 reflections [$I > 10\sigma(I)$] and are given in Table 3.

208 The SHELXL-97 software package (Sheldrick 2008) was used for refinement of the
209 Urubu fluor-elbaite crystal structure. Starting coordinates were taken from a crystal described in
210 Lussier et al. (2011b). Fully ionized scattering factors for O²⁻ were used, whereas neutral
211 scattering factors for all other atoms were used, following the findings presented in Lussier *et al.*
212 (2011b) that showed best agreement between chemical and structural data using these particular
213 scattering factors. The X-site was modeled using the Na scattering factor and the occupancy was
214 allowed to refine. The Z, T, B, O1 sites were refined using Al, Si, B and F scattering factors,

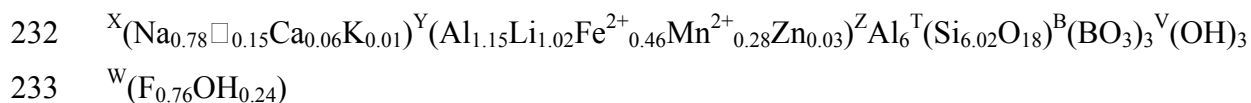
215 respectively, and were held fixed at full occupancy, following the observation that removing
216 these constraints during refinement cycles resulted in no significant deviation from full
217 occupancy at any of these sites. Chemical analysis by electron microprobe showed the *Y* site
218 occupancy to approximate $Y = [(Fe + Mn)_{1.0}Al_{1.2}Li_{0.8}]$, if the *Z*-site was set to $Z = Al_6$.
219 Accordingly, the *Y* site was refined by setting the Fe occupancy to 1.0 atoms per formula unit
220 (apfu) and allowing the remaining 2/3 of the site to refine as $Al = (2 - Li)$ apfu. The position of
221 the H atom bonded to the oxygen at the O3 position in the structure was taken from the
222 difference-Fourier map and incorporated into the refinement model; the O3-H3 bond length was
223 constrained to be 0.98 Å. Also this sample was refined twice according to the above-mentioned
224 findings of Burns et al. (1994). Table 3 lists crystal data, data collection information and
225 refinement details; Table 4 gives the fractional atomic coordinates, equivalent isotropic
226 displacement parameters; Table 5 (on deposit) contains anisotropic displacement parameters;
227 Table 6 shows selected bond lengths.

228

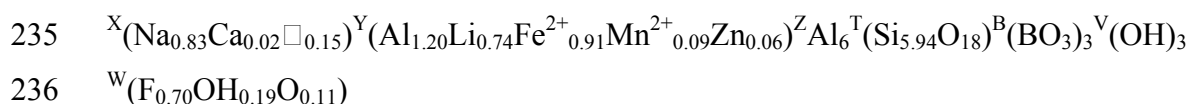
229

RESULTS AND DISCUSSION

230 In accord with the classification procedure of Henry et al. (2011), the empirical ordered
231 formula of the studied fluor-elbaite specimens can be written as (Table 1):



234 for the Cruzeiro sample and



237 for the Urubu sample.

238 These empirical formulae are consistent with the refined site-scattering values (Table 7),
239 and show ${}^Y(2Li)$ contents larger than ${}^YR^{2+}$ (divalent cations), which is typical of a XNa -, ZAl -
240 dominant tourmaline belonging to the alkali group-subgroup 2 (Henry et al. 2011). As ${}^WF >$
241 WOH , the studied samples are named fluor-elbaite, referring to the ideal formula
242 $Na(Li_{1.5}Al_{1.5})Al_6(Si_6O_{18})(BO_3)_3(OH)_3F$.

243 Observed $\langle T-O \rangle$ bond distances of Cruzeiro and Urubu fluor-elbaite (1.619 Å and 1.620
244 Å, respectively) are consistent with a *T* site fully populated by Si (MacDonald and Hawthorne
245 1995; Bosi and Lucchesi 2007). Observed $\langle Y-O \rangle$ distances of the Cruzeiro and Urubu samples

246 (2.030 Å and 2.036 Å, respectively) are in very good agreement with $\langle Y-O \rangle \sim 2.035$ Å
247 calculated for the Y populations reported above using the ionic radii of Bosi and Lucchesi
248 (2007). Compared to the value calculated for an ideal Y site populated by (Al_{1.5}Li_{1.5}) of $\langle Y-O \rangle \sim$
249 2.005 Å, these values are significantly greater due to the occurrence of the relatively large
250 cations Fe²⁺ and Mn²⁺ at Y. Furthermore, observed $\langle Z-O \rangle$ distances of the Cruzeiro and Urubu
251 samples (1.908 Å and 1.907 Å, respectively) are perfectly in line with the value 1.907 Å
252 expected for a Z site fully populated by Al (Bosi and Lucchesi 2007; Bosi 2008).

253 With respect to the ideal fluor-elbaite, the minor constituents in the empirical formulae
254 are due to various substitutions: $2R^{2+} \leftrightarrow Li + Al$ (which relates to the divalent cations); $\square +$
255 $0.5Al \leftrightarrow Na + 0.5Li$ (which relates to the vacant group); $OH \leftrightarrow F$ (which relates to the hydroxy
256 subgroup). Fluor-elbaite, besides the obvious occurrence of a solid solution with elbaite, also
257 shows relations with tsilaisite through the ideal substitution ${}^Y(Al + Li) + {}^WF \leftrightarrow 2{}^YMn^{2+} + {}^WOH$,
258 as already observed in a zoned tourmaline crystal from Elba Island by Bosi et al. (2012).
259 Comparative data for fluor-elbaite, elbaite and tsilaisite are given in Table 8.

260

261

262

ACKNOWLEDGMENTS

263 FCH is grateful to Bill Pinch for loan of the fluor-elbaite specimen from the Urubu mine.
264 AJL was supported by a PGS-D (Post-Graduate Scholarship) from the Natural Sciences and
265 Engineering Research Council of Canada; FCH was supported by a Canada Research Chair in
266 Crystallography and Mineralogy and by a Discovery grant from the Natural Sciences and
267 Engineering Research Council of Canada, and by grants from the Canada Foundation for
268 Innovation. Comments and suggestions by Darrell Henry, Alexander U. Falster, and the AE
269 Aaron Celestian are appreciated.

270
271
272
273
274
275
276
277
278
279
280
281
282
283
284
285
286
287
288
289
290
291
292
293
294
295
296
297
298
299
300
301
302
303

REFERENCES

- Agrosi, G., Bosi, F., Lucchesi, S., Melchiorre, G., and Scandale, E. (2006) Mn-tourmaline crystals from island of Elba (Italy): Growth history and growth marks. *American Mineralogist*, 91, 944-952.
- Bosi, F. (2008) Disordering of Fe²⁺ over octahedrally coordinated sites of tourmaline. *American Mineralogist*, 93, 1647-1653.
- Bosi, F. (2010) Octahedrally coordinated vacancies in tourmaline: a theoretical approach. *Mineralogical Magazine*, 74, 1037-1044.
- Bosi, F. (2011) Stereochemical constraints in tourmaline: from a short-range to a long-range structure. *Canadian Mineralogist*, 49, 17-27.
- Bosi, F. and Lucchesi, S. (2007) Crystal chemical relationships in the tourmaline group: structural constraints on chemical variability. *American Mineralogist*, 92, 1054-1063.
- Bosi, F., Balić-Žunić, T., and Surour, A.A., (2010) Crystal structure analysis of four tourmalines from the Cleopatra's Mines (Egypt) and Jabal Zalm (Saudi Arabia), and the role of Al in the tourmaline group. *American Mineralogist*, 95, 510-518.
- Bosi, F., Skogby, H., Agrosi, G., and Scandale, E. (2012) Tsilaisite, NaMn₃Al₆(Si₆O₁₈)(BO₃)₃(OH)₃OH, a new mineral species of the tourmaline supergroup from Grotta d'Oggi, San Piero in Campo, island of Elba, Italy. *American Mineralogist*, 97, 989-994.
- Burns, P.C., MacDonald, D.J., and Hawthorne, F.C. (1994) The crystal-chemistry of manganese-bearing elbaite. *Canadian Mineralogist*, 32, 31-41.
- Federico, M., Andreozzi, G.B., Lucchesi, S., Graziani, G., and César-Mendes, J. (1998) Crystal chemistry of tourmalines. I. Chemistry, compositional variations and coupled substitutions in the pegmatite dikes of the Cruzeiro mine, Minas Gerais, Brazil. *Canadian Mineralogist*, 36, 415-431.
- Foit, F.F. Jr. (1989) Crystal chemistry of alkali-deficient schorl and tourmaline structural relationships. *American Mineralogist*, 74, 422-431.
- Jernberg, P. and Sundqvist, T. (1983) A versatile Mössbauer analysis program. Uppsala University, Institute of Physics (UUIP-1090).
- Hawthorne, F.C. (1996) Structural mechanisms for light-element variations in tourmaline. *Canadian Mineralogist*, 34, 123-132.
- Hawthorne, F.C. (2002) Bond-valence constraints on the chemical composition of tourmaline. *Canadian Mineralogist*, 40, 789-797.

- 304 Hawthorne, F.C. and Henry, D. (1999) Classification of the minerals of the tourmaline group.
305 European Journal of Mineralogy, 11, 201-215.
- 306 Henry, D.J., Dutrow, B.L. (2011) The incorporation of fluorine in tourmaline: Internal
307 crystallographic controls or external environmental influences? Canadian Mineralogist,
308 49, 41-56.
- 309 Henry, D.J., Novák, M., Hawthorne, F.C., Ertl, A., Dutrow, B., Uher, P., and Pezzotta, F.
310 (2011) Nomenclature of the tourmaline supergroup minerals. American Mineralogist,
311 96, 895-913.
- 312 Holland, T.J.B. and Redfern, S.A.T. (1997) Unit cell refinement from powder diffraction
313 data: the use of regression diagnostics. Mineralogical Magazine, 61, 65-77.
- 314 Lussier, A.J., Aguiar, P.M., Michaelis, V.K., Kroeker, S., Herwig, S., Abdu, Y., and
315 Hawthorne, F.C. (2008) Mushroom elbaite from the Kat Chay mine, Momeik, near
316 Mogok, Myanmar: I. Crystal chemistry by SREF, EMPA, MAS NMR and Mössbauer
317 spectroscopy. Mineralogical Magazine, 72, 747-761.
- 318 Lussier A.J., Hawthorne F.C., Aguiar P.M., Michaelis V.K., and Kroeker S. (2011a) Elbaite-
319 liddicoatite from Black Rapids glacier, Alaska. Periodico di Mineralogia, 80, 57-73.
- 320 Lussier, A.J., Abdu, Y. Hawthorne, F.C., Michaelis, V.K., Aguiar, P.M., and Kroeker, S.
321 (2011b) Oscillatory zoned liddicoatite from Anjanabonoina, central Madagascar. I.
322 Crystal chemistry and structure by SREF and ^{11}B and ^{27}Al MAS NMR spectroscopy.
323 Canadian Mineralogist, 49, 63-88.
- 324 Mandarino, J.A. (1976) The Gladstone-Dale relationship. Part I: derivation of new constants.
325 Canadian Mineralogist, 14, 498-502.
- 326 Mandarino, J.A. (1981) The Gladstone-Dale relationship. Part IV: the compatibility concept
327 and its application. Canadian Mineralogist, 19, 441-450.
- 328 MacDonald, D.J. and Hawthorne, F.C. (1995) The crystal chemistry of Si = Al substitution in
329 tourmaline. Canadian Mineralogist, 33, 849-858.
- 330 Novák, M., Povondra, P., and Selway, J.B. (2004) Schorl-oxy-schorl to dravite-oxy-dravite
331 tourmaline from granitic pegmatites; examples from the Moldanubicum, Czech
332 Republic. European Journal of Mineralogy, 16, 323-333.
- 333 Novák M., Škoda P., Filip J., Macek I., and Vaculovič T. (2011) Compositional trends in
334 tourmaline from intragranitic NYF pegmatites of the Třebíč Pluton, Czech Republic;
335 electron microprobe, Mössbauer and LA-ICP-MS study. Canadian Mineralogist, 49,
336 359-380.

- 337 Rancourt, D.G. (1994) Mössbauer spectroscopy of minerals. I. Inadequacy of Lorentzian-line
338 doublets in fitting spectra arising from quadrupole splitting distributions. *Physics and*
339 *Chemistry of Minerals*, 21, 244-249.
- 340 Rancourt, D.G., and Ping, J.Y. (1991) Voigt-based methods for arbitrary shape static
341 hyperfine parameter distributions in Mössbauer spectroscopy. *Nuclear Instruments and*
342 *Methods in Physics Research*, B58, 85-97.
- 343 Rancourt, D.G., McDonald, A.M., Lalonde, A.E., and Ping, Y.J. (1993) Mössbauer absorber
344 thicknesses for accurate site populations in Fe-bearing minerals *American Mineralogist*,
345 78, 1-7.
- 346 Sheldrick, G.M. (1996) SADABS, Absorption Correction Program. University of Göttingen,
347 Germany.
- 348 Sheldrick, G.M. (2008) A short history of SHELX. *Acta Crystallographica*, A64, 112-122.
- 349 van Hinsberg, V.J. and Schumacher, J.C. (2011) Tourmaline as a petrogenetic indicator
350 mineral in the Haut-Allier metamorphic suite, Massif Central, France. *Canadian*
351 *Mineralogist*, 49, 177-194.
- 352 van Hinsberg, V.J., Henry, D.J., and Marschall, H.R. (2011) Tourmaline: an ideal indicator of
353 its host environment. *Canadian Mineralogist*, 49, 1-16.

354 **LIST OF TABLES**

355

356 **TABLE 1.** Chemical composition of fluor-elbaite.

357 **TABLE 2.** X-ray powder diffraction data for fluor-elbaite.

358 **TABLE 3.** Single crystal X-ray diffraction data details for fluor-elbaite.

359 **TABLE 4.** Fractional atomic coordinates (x,y,z) and equivalent (U_{eq}) displacement parameters
360 for fluor-elbaite (\AA^2).

361 **TABLE 5.** (on deposit). Anisotropic displacement parameters (\AA^2) for non-hydrogen atoms in
362 the two analyzed fluor-elbaite samples.

363 **TABLE 6.** Selected bond lengths (\AA) in fluor-elbaite.

364 **TABLE 7.** Site populations and scattering factors in fluor-elbaite.

365 **TABLE 8.** Comparative data for fluor-elbaite, elbaite and tsilaisite.

366

367

368 **LIST OF FIGURES AND FIGURE CAPTIONS**

369

370 **FIGURE 1.** Photos of the holotype fragment of fluor-elbaite from Cruzeiro (Brazil) in
371 reflected (a) and transmitted (b) light.

372 **FIGURE 2.** Photos of a representative crystal of fluor-elbaite (unknown locality) in reflected
373 (a) and transmitted (b) light.

374 **FIGURE 3.** Room-temperature Mössbauer spectrum of fluor-elbaite (Cruzeiro), fitted with
375 three doublets (thin lines) assigned to Fe^{2+} (centroid shifts: 1.07, 1.13, 1.24 mm/s;
376 quadrupole splittings: 2.41, 2.29, 1.82 mm/s, respectively, relative to α -Fe foil).
377 Thick line denotes summed spectrum.

378

379

380

TABLE 1. Chemical composition of fluor-elbaite

Sample	Cruzeiro		Urubu	
	Average	Probe standard	Average	Probe standard
SiO ₂ wt%	37.48(18)	Wollastonite	36.70(17)	Diopside
B ₂ O ₃	10.83(56)*	Elbaite	10.73(6)‡	
Al ₂ O ₃	37.81(18)	Corundum	37.73(12)	Andalusite
FeO	3.39(10)†	Magnetite	6.69(8)†	Fayalite
MnO	2.09(9)	Metallic Mn	0.64(3)	Spessartine
ZnO	0.27(9)	Metallic Zn	0.53(4)	Gahnite
CaO	0.34(5)	Wollastonite	0.10(1)	Diopside
Na ₂ O	2.51(5)	Jadeite	2.65(4)	Albite
K ₂ O	0.06(2)	Orthoclase	bdl	Orthoclase
Li ₂ O	1.58(10)*	Elbaite	1.14(5)‡	
F	1.49(10)	Fluorophlogopite	1.37(11)	Fluororiebeckite
H ₂ O	3.03‡		2.95(5)*	Elbaite
-O = F	-0.63		-0.58	
Total	100.25		100.67	
Atomic proportions normalized to 31 anions				
Si apfu	6.02(5)		5.94(2)	
B	3.0(1)		3.0(1)	
Al	7.15(6)		7.20(4)	
Fe ²⁺	0.46(1)		0.91(1)	
Mn ²⁺	0.28(1)		0.09(1)	
Zn	0.03(1)		0.06(1)	
Ca	0.06(1)		0.02(1)	
Na	0.78(2)		0.83(1)	
K	0.012(4)		-	
Li	1.02(6)		0.74(3)	
F	0.76(5)		0.70(5)	
OH	3.24		3.19(4)	

* Measured by secondary-ion mass spectrometry.

† Measured as Fe²⁺ by Mössbauer spectroscopy.

‡ Calculated by stoichiometry. In detail, the B₂O₃ and Li₂O contents for the Urubu sample were calculated on the same basis of B = 3 apfu and Li apfu = 9 - Σ(Y + Z); the H₂O content for the Cruzeiro sample was calculated on the basis of OH + F = 4 apfu.

Notes: Standard errors for the atomic proportions (in brackets) were calculated by error-propagation theory. Ti and Mg were found to be below their respective detection limits (0.03 wt%). bdl = below detection limits, apfu = atoms per formula unit.

TABLE 2. X-ray powder diffraction data for fluor-elbaite

Cruzeiro				Urubu			
$I_{(\text{meas})}$ %	hkl	$d_{(\text{meas})}$ Å	$d_{(\text{calc})}$ Å	$I_{(\text{meas})}$ %	hkl	$d_{(\text{meas})}$ Å	$d_{(\text{calc})}$ Å
17	1 0 1	6.318	6.326	4	$\bar{1} 2 0$	7.977	7.958
18	0 2 1	4.950	4.950	32	$\bar{1} 1 1$	6.332	6.326
12	0 3 0	4.587	4.589	32	0 2 1	4.957	4.952
49	2 1 1	4.200	4.202	20	0 3 0	4.598	4.594
58	2 2 0	3.974	3.974	66	$\bar{2} 3 1$	4.206	4.204
67	0 1 2	3.447	3.448	78	$\bar{2} 4 0$	3.977	3.979
14	1 3 1	3.365	3.365	60	0 1 2	3.449	3.447
14	4 1 0	3.004	3.004	17	$\bar{1} 4 1$	3.369	3.368
92	1 2 2	2.939	2.939	5	$\bar{4} 4 1$	3.101	3.102
6	3 2 1	2.885	2.887	16	$\bar{1} 5 0$	3.006	3.008
8	3 1 2	2.604	2.604	81	$\bar{1} 3 2$	2.939	2.939
100	0 5 1	2.568	2.568	100	0 5 1	2.569	2.571
16	0 0 3	2.374	2.374	2	0 4 2	2.478	2.476
22	5 1 1	2.336	2.336	3	$\bar{2} 6 1$	2.447	2.446
11	5 0 2	2.178	2.178	27	0 0 3	2.367	2.373
15	4 3 1	2.157	2.157		$\bar{2} 5 2$	2.367	2.364
17	0 3 3	2.109	2.109	24	$\bar{5} 6 1$	2.342	2.338
27	2 2 3	2.038	2.038	4	0 6 0	2.295	2.297
57	1 5 2	2.031	2.031	22 B	$\bar{5} 5 2$	2.161*	
7	1 6 1	2.014	2.014		$\bar{4} 7 1$	2.161*	
3	4 4 0	1.986	1.987	24	$\bar{3} 3 3$	2.107	2.109
23	3 4 2	1.910	1.910		0 3 3	2.107	2.109
8	1 4 3	1.862	1.863		$\bar{4} 6 2$	2.107	2.102
10	1 0 4	1.767	1.766	69	$\bar{2} 4 3$	2.034	2.038
31	0 6 3	1.650	1.650		$\bar{1} 6 2$	2.034	2.032
21	5 5 0	1.590	1.590	5	$\bar{4} 8 0$	1.990	1.989
8	4 5 2	1.581	1.580	43	$\bar{3} 7 2$	1.911	1.912
24	0 5 4	1.495	1.495	9	$\bar{1} 5 3$	1.862	1.863
32	6 4 2	1.445	1.444	12	$\bar{6} 8 1$	1.847	1.846
9	0 1 5	1.417	1.417	10	$\bar{3} 6 3$	1.768	1.769
11	6 5 1	1.414	1.414		$\bar{1} 1 4$	1.768	1.765
23	4 3 4	1.399	1.399	4	0 2 4	1.723	1.723
					$\bar{5} 8 2$	1.723	1.723
				4	$\bar{2} 8 2$	1.684	1.684
				28 B	$\bar{6} 6 3$	1.649	1.651
					0 6 3	1.649	1.651
				24 B	$\bar{2} 9 1$	1.639	1.639
				23 B	$\bar{5} 10 0$	1.590	1.592
				4B	$\bar{4} 10 1$	1.545*	
					0 9 0	1.545*	
				6B	$\bar{7} 9 2$	1.522*	
					$\bar{7} 10 1$	1.522*	
				12	0 5 4	1.496	1.495

Notes: $I_{(\text{meas})}$ = measured intensity, $d_{(\text{meas})}$ = measured interplanar spacing; $d_{(\text{calc})}$ = calculated interplanar spacing; hkl = reflection indices. Estimated errors in $d_{(\text{meas})}$ -spacing range from 0.01 Å for large d -values to 0.001 Å for small d -values.

*Not used in refinement; B = broad.

TABLE 3. Single crystal X-ray diffraction data details for fluor-elbaite

	Cruzeiro		Urubu	
Crystal size (mm)	0.30 × 0.32 × 0.33		0.14 × 0.15 × 0.10	
Unit-cell parameter <i>a</i> (Å)	15.8933(2)		15.9083(6)	
Unit-cell parameter <i>c</i> (Å)	7.1222(1)		7.1229(3)	
Unit-cell volume (Å ³)	1558.02(4)		1561.12(19)	
Range for data collection, 2θ (°)	5 - 81		5 - 60	
Reciprocal space range <i>hkl</i>	-28 ≤ <i>h</i> ≤ 28		-22 ≤ <i>h</i> ≤ 22	
	-28 ≤ <i>k</i> ≤ 20		-22 ≤ <i>k</i> ≤ 22	
	-12 ≤ <i>l</i> ≤ 12		-9 ≤ <i>l</i> ≤ 10	
Total number of frames	4830		4580	
Set of measured reflections	12117		7994	
Unique reflections, <i>R</i> _{int} (%)	2279, 2.11		4617, 2.22	
Absorption correction method	SADABS		SADABS	
Refinement method	Full-matrix least-squares on <i>F</i> ²		Full-matrix least-squares on <i>F</i> ²	
Structural refinement program	SHELXL-97		SHELX-97	
	<u>Standard SREF</u>	<u>Split-site SREF</u>	<u>Standard SREF</u>	<u>Split-site SREF</u>
Extinction coefficient	0.0042(2)	0.0041(2)	0.0036(2)	0.0034(2)
Flack parameter	0.22(1)	0.22(1)	0.01(3)	0.02(3)
w <i>R</i> 2 (%)	4.40	3.75	4.58	4.29
<i>R</i> 1 (%) all data	1.87	1.50	1.90	1.75
<i>R</i> 1 (%) for <i>I</i> > 2σ _{<i>I</i>}	1.84	1.48	1.90	1.75
GooF	1.070	1.094	1.136	1.175
Diff. Peaks (±e ⁻ /Å ³)	2.25; -1.06	0.71; -0.48	0.87; -0.42	0.32; -0.30

Notes: Standard and Split-site SREF denote, respectively, structural refinements carried out with the O1 site at (0,0,*z*) and the O2 site at (*x*,2*x*,*z*), and with O1 at (*x*,2*x*,*z*) and O2 at (*x*,*y*,*z*) to allow for positional disorder, as indicated by the high *U*_{eq} values (Burns et al. 1994). *R*_{int} = merging residual value; *R*1 = discrepancy index, calculated from *F*-data; w*R*2 = weighted discrepancy index, calculated from *F*²-data; GooF = goodness of fit; Diff. Peaks = maximum and minimum residual electron density. Radiation, Mo-*K*α = 0.71073 Å. Data collection temperature = 293 K. Space group *R*3*m*; *Z* = 3.

TABLE 4. Fractional atomic coordinates (x,y,z) and equivalent (U_{eq}) displacement parameters for fluor-elbaite (\AA^2)

Site	Sample	Standard SREF				Split-site SREF			
		x	y	z	U_{eq}	x	y	z	U_{eq}
X	Cruzeiro	0	0	0.2362(2)	0.0215(4)	0	0	0.23648(16)	0.0205(3)
	Urubu	0	0	0.2361(4)	0.0280(9)	0	0	0.2364(3)	0.0261(8)
Y	Cruzeiro	0.12374(3)	$x/2$	0.62863(7)	0.00950(10)	0.12377(3)	$x/2$	0.62862(6)	0.00948(8)
	Urubu	0.12422(5)	$x/2$	0.62764(12)	0.0104(2)	0.12424(5)	$x/2$	0.62767(11)	0.0105(2)
Z	Cruzeiro	0.29746(2)	0.26065(2)	0.61125(5)	0.00613(5)	0.297451(16)	0.260633(17)	0.61131(4)	0.00612(4)
	Urubu	0.29770(4)	0.26081(4)	0.61147(11)	0.00787(12)	0.29768(4)	0.26081(4)	0.61157(10)	0.00779(11)
B	Cruzeiro	0.10946(5)	$2x$	0.45531(19)	0.00651(18)	0.10945(4)	$2x$	0.45525(15)	0.00665(15)
	Urubu	0.10966(11)	$2x$	0.4553(4)	0.0087(5)	0.10948(10)	$2x$	0.4553(4)	0.0092(4)
T	Cruzeiro	0.191971(16)	0.189959(17)	0	0.00505(4)	0.191977(13)	0.189963(14)	0	0.00495(4)
	Urubu	0.19200(3)	0.18999(3)	0	0.00659(11)	0.19200(3)	0.18999(3)	0	0.00646(10)
O1	Cruzeiro	0	0	0.7841(4)	0.0579(9)	0.02288(13)	$x/2$	0.7847(3)	0.0138(4)*
	Urubu	0	0	0.7849(6)	0.0596(14)	0.0238(3)	$x/2$	0.7854(5)	0.0142(10)*
O2	Cruzeiro	0.06070(4)	$2x$	0.48468(17)	0.0168(2)	0.06993(9)	0.12159(7)	0.48469(13)	0.00845(18)*
	Urubu	0.06092(7)	$2x$	0.4845(3)	0.0183(5)	0.0518(2)	0.9299(2)	0.4846(3)	0.0103(5)*
O3	Cruzeiro	0.26834(9)	$x/2$	0.50937(14)	0.01039(16)	0.26853(7)	$x/2$	0.50940(11)	0.01020(13)
	Urubu	0.26872(15)	$x/2$	0.5096(3)	0.0111(4)	0.26888(14)	$x/2$	0.5097(2)	0.0110(3)
O4	Cruzeiro	0.09316(4)	$2x$	0.07182(14)	0.00815(14)	0.09316(3)	$2x$	0.07170(11)	0.00815(12)
	Urubu	0.09316(7)	$2x$	0.0709(3)	0.0099(4)	0.09313(6)	$2x$	0.0709(2)	0.0100(3)
O5	Cruzeiro	0.18650(8)	$x/2$	0.09399(13)	0.00817(14)	0.18644(6)	$x/2$	0.09399(11)	0.00820(12)
	Urubu	0.18676(15)	$x/2$	0.0938(3)	0.0103(3)	0.18668(13)	$x/2$	0.0938(2)	0.0105(3)
O6	Cruzeiro	0.19679(5)	0.18654(5)	0.77568(9)	0.00727(10)	0.19673(4)	0.18650(4)	0.77569(8)	0.00739(8)
	Urubu	0.19723(9)	0.18700(9)	0.77565(19)	0.0089(2)	0.19722(8)	0.18699(8)	0.77565(18)	0.0089(2)
O7	Cruzeiro	0.28573(5)	0.28582(5)	0.08016(9)	0.00635(9)	0.28571(4)	0.28581(4)	0.08019(7)	0.00630(8)
	Urubu	0.28570(9)	0.28587(9)	0.08034(18)	0.0079(2)	0.28568(8)	0.28588(8)	0.08039(17)	0.0079(2)
O8	Cruzeiro	0.20986(5)	0.27041(5)	0.44124(10)	0.00762(10)	0.20983(4)	0.27046(4)	0.44134(8)	0.00755(8)
	Urubu	0.21002(10)	0.27051(10)	0.4413(2)	0.0095(3)	0.20996(9)	0.27053(9)	0.44143(18)	0.0095(2)
H3	Cruzeiro	0.2553(19)	0.1277(9)	0.390(4)	0.016*	0.2496(15)	0.1248(7)	0.394(3)	0.015*
	Urubu	0.263(3)	0.1316(13)	0.3724(5)	0.015*	0.262(2)	0.1308(12)	0.3729(5)	0.015*

Notes: Standard and Split-site SREF denote, respectively, structural refinements carried out with the O1 site at (0,0, z) and the O2 site at ($x,2x,z$), and with O1 at ($x,x/2,z$) and O2 at (x,y,z) to allow for positional disorder, as indicated by the high U_{eq} values (Burns et al. 1994).

* Isotropic displacement parameter

TABLE 5. (on deposit). Anisotropic displacement parameters (\AA^2) for non-hydrogen atoms in the two analyzed fluor-elbaite samples.

Site	Sample	Standard SREF						Split-site SREF					
		U^{11}	U^{22}	U^{33}	U^{23}	U^{13}	U^{12}	U^{11}	U^{22}	U^{33}	U^{23}	U^{13}	U^{12}
X	Cruzeiro	0.0247(5)	0.0247(5)	0.0150(6)	0	0	0.0124(3)	0.0233(4)	0.0233(4)	0.0149(5)	0	0	0.0116(2)
	Urubu	0.0310(11)	0.0310(11)	0.0219(14)	0	0	0.0155(5)	0.029(1)	0.029(1)	0.0212(12)	0	0	0.0143(5)
Y	Cruzeiro	0.00938(17)	0.00812(13)	0.01143(17)	-0.00053(6)	-0.00107(11)	0.00469(8)	0.00924(14)	0.00799(11)	0.01162(14)	-0.00057(5)	-0.00114(9)	0.00462(7)
	Urubu	0.0102(4)	0.0089(3)	0.0125(4)	-0.00057(11)	-0.0011(2)	0.00510(18)	0.0101(3)	0.0088(3)	0.0129(3)	-0.00058(10)	-0.0012(2)	0.00502(16)
Z	Cruzeiro	0.00620(11)	0.00732(11)	0.00530(9)	0.00059(8)	0.00008(8)	0.00369(9)	0.00626(9)	0.00734(9)	0.00525(7)	0.00060(6)	0.00007(6)	0.00378(7)
	Urubu	0.0079(2)	0.0093(3)	0.0070(2)	0.00068(19)	0.00048(18)	0.0048(2)	0.0079(2)	0.0093(2)	0.0067(2)	0.00076(17)	0.00047(16)	0.00472(18)
B	Cruzeiro	0.0069(3)	0.0058(4)	0.0064(4)	0.0007(3)	0.00036(17)	0.0029(2)	0.0071(3)	0.0062(4)	0.0064(3)	0.0004(3)	0.00020(14)	0.00311(18)
	Urubu	0.0093(9)	0.0088(12)	0.0079(11)	0.0008(9)	0.0004(4)	0.0044(6)	0.0098(8)	0.0108(11)	0.0073(10)	-0.0000(8)	-0.0000(4)	0.0054(5)
T	Cruzeiro	0.00502(9)	0.00484(9)	0.00526(8)	-0.00017(7)	0.00007(7)	0.00245(7)	0.00483(7)	0.00480(7)	0.00522(6)	-0.00018(6)	0.00011(6)	0.00240(6)
	Urubu	0.0066(2)	0.0062(2)	0.0069(2)	-0.00023(16)	0.00002(17)	0.00314(16)	0.0063(2)	0.00612(19)	0.00689(18)	-0.00027(14)	0.00008(15)	0.00302(14)
O1	Cruzeiro	0.0812(15)	0.0812(15)	0.0113(9)	0	0	0.0406(8)	Isotropic					
	Urubu	0.084(2)	0.084(2)	0.0113(17)	0	0	0.0419(12)	Isotropic					
O2	Cruzeiro	0.0264(5)	0.0044(4)	0.0122(4)	0.0009(3)	0.00043(15)	0.00222(18)	Isotropic					
	Urubu	0.0275(9)	0.0275(9)	0.014(1)	-0.0001(4)	0.0001(4)	0.024(1)	Isotropic					
O3	Cruzeiro	0.0201(5)	0.0093(2)	0.0054(3)	-0.00015(15)	-0.0003(3)	0.0101(2)	0.0198(4)	0.0092(2)	0.0052(2)	-0.00016(12)	-0.0003(2)	0.00988(19)
	Urubu	0.0207(10)	0.0103(6)	0.0058(8)	-0.0001(4)	-0.0002(7)	0.0104(5)	0.0206(9)	0.0104(6)	0.0053(7)	0.0000(3)	0.0000(6)	0.0103(5)
O4	Cruzeiro	0.0066(2)	0.0120(4)	0.0076(3)	-0.0007(3)	-0.00037(14)	0.00601(19)	0.00655(19)	0.0119(3)	0.0078(2)	-0.0011(2)	-0.00054(12)	0.00594(16)
	Urubu	0.0086(6)	0.0123(9)	0.0100(8)	-0.0003(7)	-0.0001(3)	0.0062(5)	0.0086(6)	0.0131(8)	0.0099(7)	-0.0006(6)	-0.0003(3)	0.0065(4)
O5	Cruzeiro	0.0129(4)	0.0062(2)	0.0077(3)	0.00045(14)	0.0009(3)	0.0064(2)	0.0133(3)	0.00624(18)	0.0075(3)	0.00030(11)	0.0006(2)	0.00663(16)
	Urubu	0.014(9)	0.0083(6)	0.0103(8)	0.0004(3)	0.0008(7)	0.0071(5)	0.0147(9)	0.0088(5)	0.0100(8)	0.0002(3)	0.0004(6)	0.0074(4)
O6	Cruzeiro	0.0070(2)	0.0083(2)	0.0049(2)	-0.00008(18)	0.00047(17)	0.0026(2)	0.00704(19)	0.0087(2)	0.00487(17)	-0.00028(15)	0.00028(14)	0.00274(16)
	Urubu	0.0084(6)	0.0099(6)	0.0063(5)	0.0002(4)	0.0003(4)	0.0030(5)	0.0084(5)	0.0104(5)	0.0061(5)	0.0000(4)	0.0001(4)	0.0034(4)
O7	Cruzeiro	0.0056(2)	0.0056(2)	0.0061(2)	-0.00107(17)	0.00043(17)	0.00138(18)	0.00556(18)	0.00548(18)	0.00601(18)	-0.00112(14)	0.00038(14)	0.00137(15)
	Urubu	0.0075(6)	0.0068(5)	0.0076(5)	-0.0012(4)	0.0001(4)	0.0023(5)	0.0073(5)	0.0072(5)	0.0074(5)	-0.0010(4)	0.0004(4)	0.0023(4)
O8	Cruzeiro	0.0056(2)	0.0103(3)	0.0077(2)	0.00325(19)	0.00092(18)	0.0045(2)	0.00556(19)	0.0103(2)	0.00750(17)	0.00329(15)	0.00114(15)	0.00449(17)
	Urubu	0.0077(6)	0.0115(6)	0.0108(6)	0.003(5)	0.0009(5)	0.0058(5)	0.0075(5)	0.0117(6)	0.0105(5)	0.0028(4)	0.0009(4)	0.0056(5)

Notes: Standard and Split-site SREF denote, respectively, structural refinements carried out with the O1 site at (0,0,z) and the O2 site at (x,2x,z), and with O1 at (x,x/2,z) and O2 at (x,y,z) to allow for positional disorder, as indicated by the high U_{eq} values (Burns et al. 1994).

TABLE 6. Selected bond lengths (Å) in fluor-elbaite

	Standard SREF	
	Cruzeiro	Urubu
X-O2 (× 3)	2.4340(15)	2.439(3)
X-O5 (× 3)	2.7595(11)	2.765(2)
X-O4 (× 3)	2.8190(12)	2.824(2)
<X-O>	2.671	2.677
Y-O2 (× 2)	1.9743(8)	1.978(1)
Y-O6 (× 2)	2.0175(7)	2.025(1)
Y-O1	2.0312(15)	2.046(2)
Y-O3	2.1640(12)	2.161(2)
<Y-O>	2.030	2.036
*Y-O1	1.7788(19)	1.783(4)
*Y-O2 (× 2)	1.8696(11)	1.872(3)
*Y-O6 (× 2)	2.0168(6)	2.025(1)
*Y-O2 (× 2)	2.0862(12)	2.090(3)
*Y-O3	2.1658(10)	2.163(2)
*Y-O1 (× 2)	2.1848(14)	2.204(3)
Z-O6	1.8532(7)	1.850(1)
Z-O7	1.8821(7)	1.881(1)
Z-O8	1.8848(7)	1.882(1)
Z-O8'	1.9091(7)	1.912(1)
Z-O7	1.9548(7)	1.955(1)
Z-O3	1.9624(5)	1.964(1)
<Z-O>	1.9077	1.907
B-O2	1.3585(18)	1.361(3)
B-O8 (× 2)	1.3858(10)	1.388(2)
<B-O>	1.377	1.379
T-O6	1.6017(7)	1.602(1)
T-O7	1.6116(7)	1.613(1)
T-O4	1.6249(4)	1.625(1)
T-O5	1.6384(5)	1.639(1)
<T-O>	1.6192	1.620
O3-H3	0.87(3)	0.98**

* Bond lengths relative to the split-site SREF (see Table 4).
 As for the other bond lengths, they are statistically equals to
 the corresponding ones of the standard SREF.

**Fixed during refinement

TABLE 7. Site populations and scattering factors in fluor-elbaite.

Site	Sample	Site population (apfu)	Site scattering (epfu)	
			Refined	Calculated
<i>X</i>	Cruzeiro	0.78 Na + 0.06 Ca + 0.15 □ + 0.01 K	10.18(7)	10.00
	Urubu	0.83 Na + 0.02 Ca + 0.15 □	10.0(1)	9.6
<i>Y</i>	Cruzeiro	1.02 Li + 0.28 Mn ²⁺ + 0.46 Fe ²⁺ + 1.15 Al + 0.03 Zn	39.2(1)	38.7
	Urubu	0.74 Li + 0.09 Mn ²⁺ + 0.91 Fe ²⁺ + 1.20 Al + 0.06 Zn	44.1(2)	45.5
<i>Z</i>	Cruzeiro	6 Al	78*	78
	Urubu	6 Al	78*	78
<i>T</i>	Cruzeiro	6 Si	84*	84
	Urubu	6 Si	84*	84
<i>B</i>	Cruzeiro	3 B	15*	15
	Urubu	3 B	15*	15
O3 (≡ V)	Cruzeiro	3 (OH)	24*	24
	Urubu	3 (OH)	24*	24
O1 (≡ W)	Cruzeiro	0.24 (OH) + 0.76 F	9*	8.76
	Urubu	0.19 (OH) + 0.70 F + 0.11 O ²⁻	9*	8.7

*Fixed in the final stages of refinement.

apfu = atoms per formula unit; epfu = electrons per formula unit

TABLE 8. Comparative data for fluor-elbaite, elbaite and tsilaisite.

	Fluor-elbaite		Elbaite	Tsilaisite
	Cruzeiro	Urubu		
<i>a</i> (Å)	15.8933(2)	15.9083(6)	15.86	15.9461(5)
<i>c</i>	7.1222(1)	7.1229(3)	7.11	7.1380(3)
<i>V</i> (Å ³)	1558.02(4)	1561.12(19)	1548.8	1571.87(12)
Space group	<i>R3m</i>	<i>R3m</i>	<i>R3m</i>	<i>R3m</i>
Optic sign	Uniaxial (–)	Uniaxial (–)	Uniaxial (–)	Uniaxial (–)
ω	1.640(5)	1.648(2)	1.633	1.645(5)
ϵ	1.625(5)	1.629(2)	1.615	1.625(5)
Colour	Blue-green	Blue-green	Colorless, pink, green, grey-black	Greenish yellow
Pleochroism	O = green E = pale green	O = bluish green E = pale green	None to very pale shades of pink to green to grey	O = pale greenish yellow E = pale greenish yellow
Reference	This work	This work	www.mindat.org	Bosi et al. (2012)

FIGURE 1A

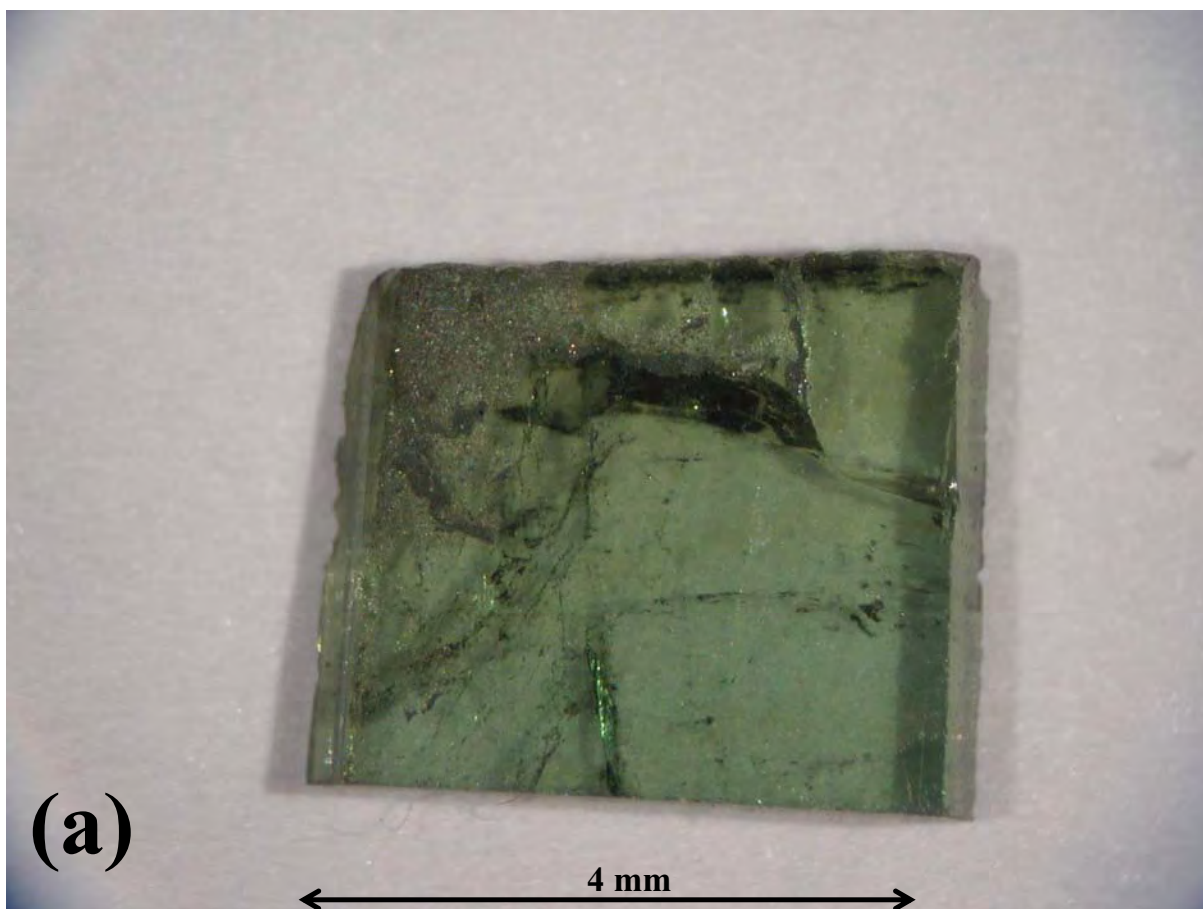


FIGURE 1B

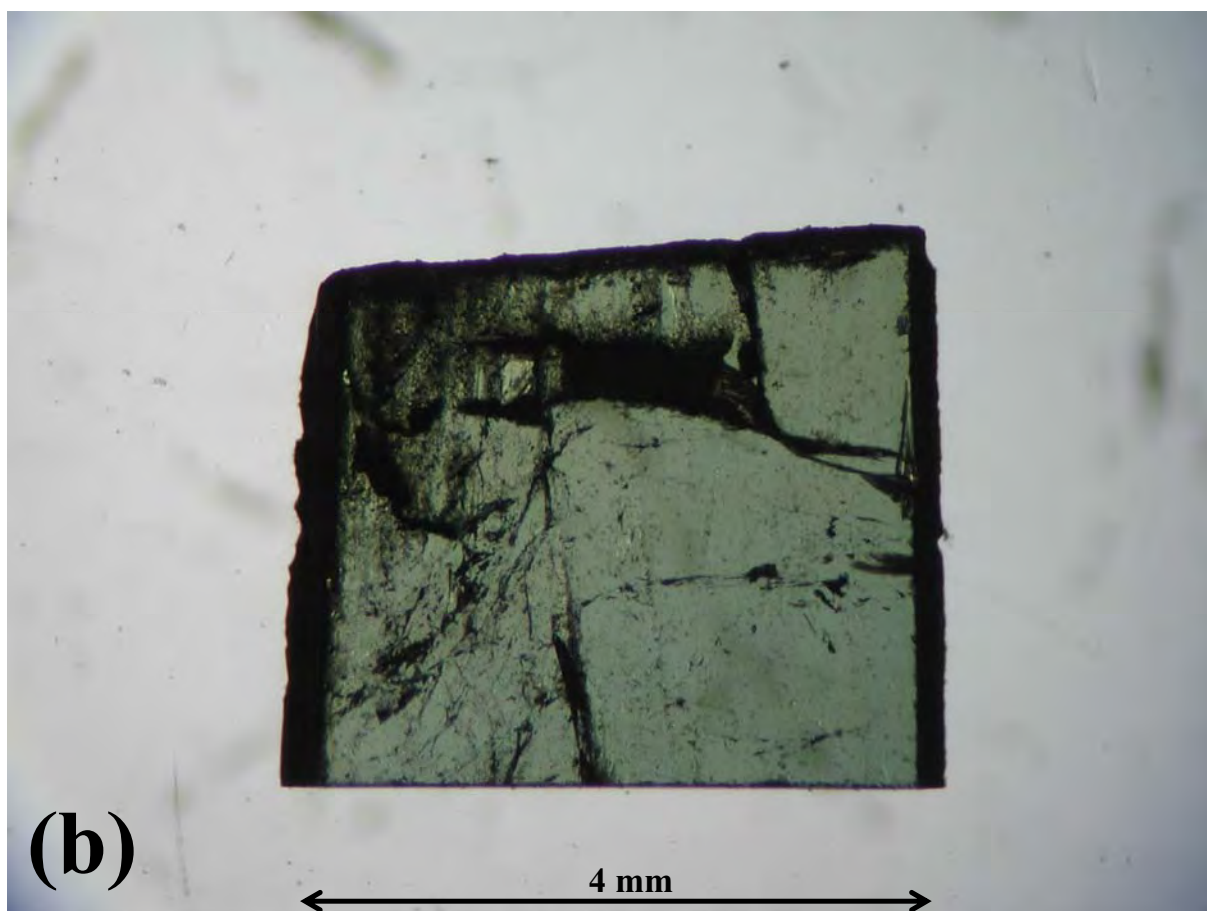


FIGURE 2A

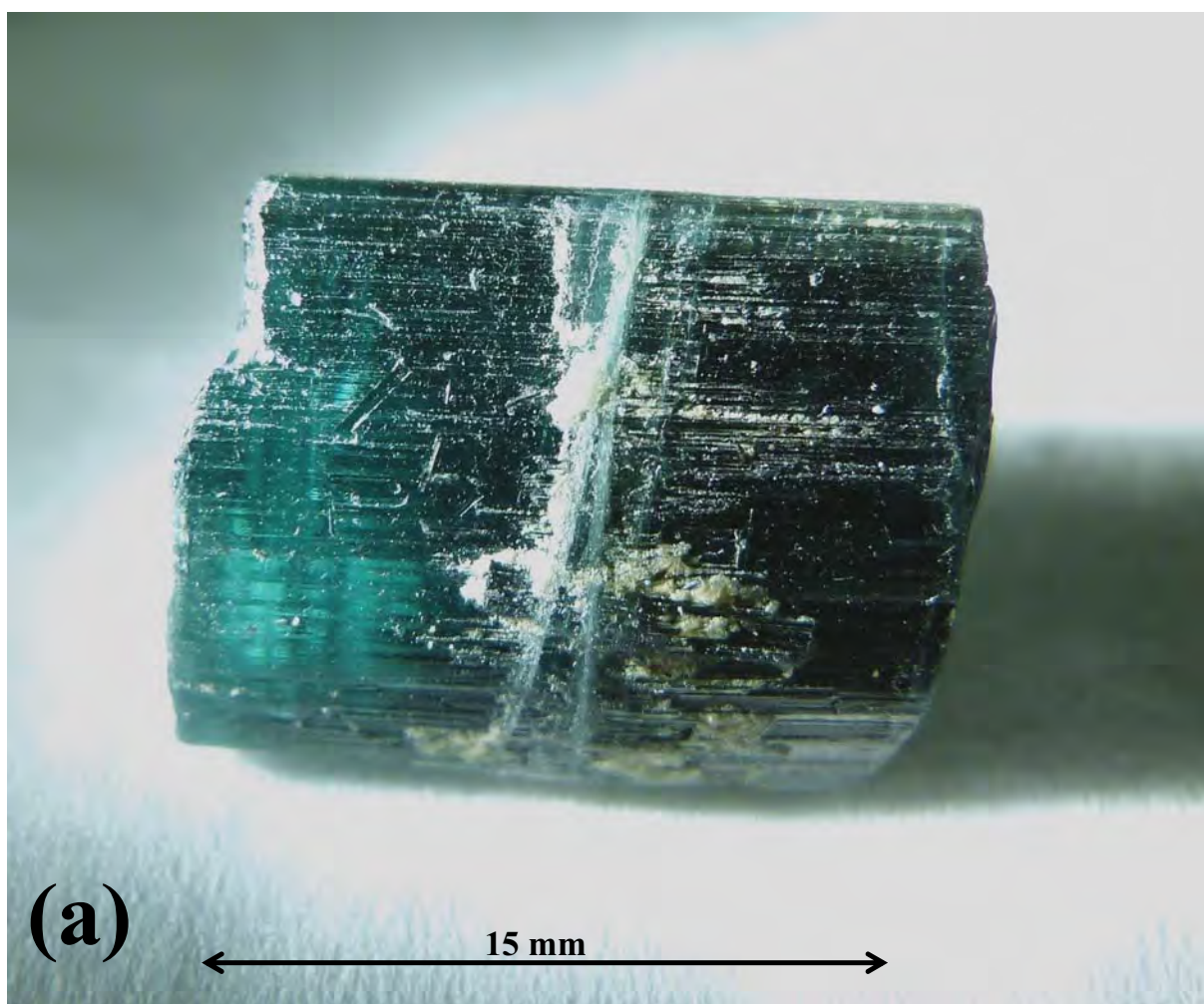


FIGURE 2B

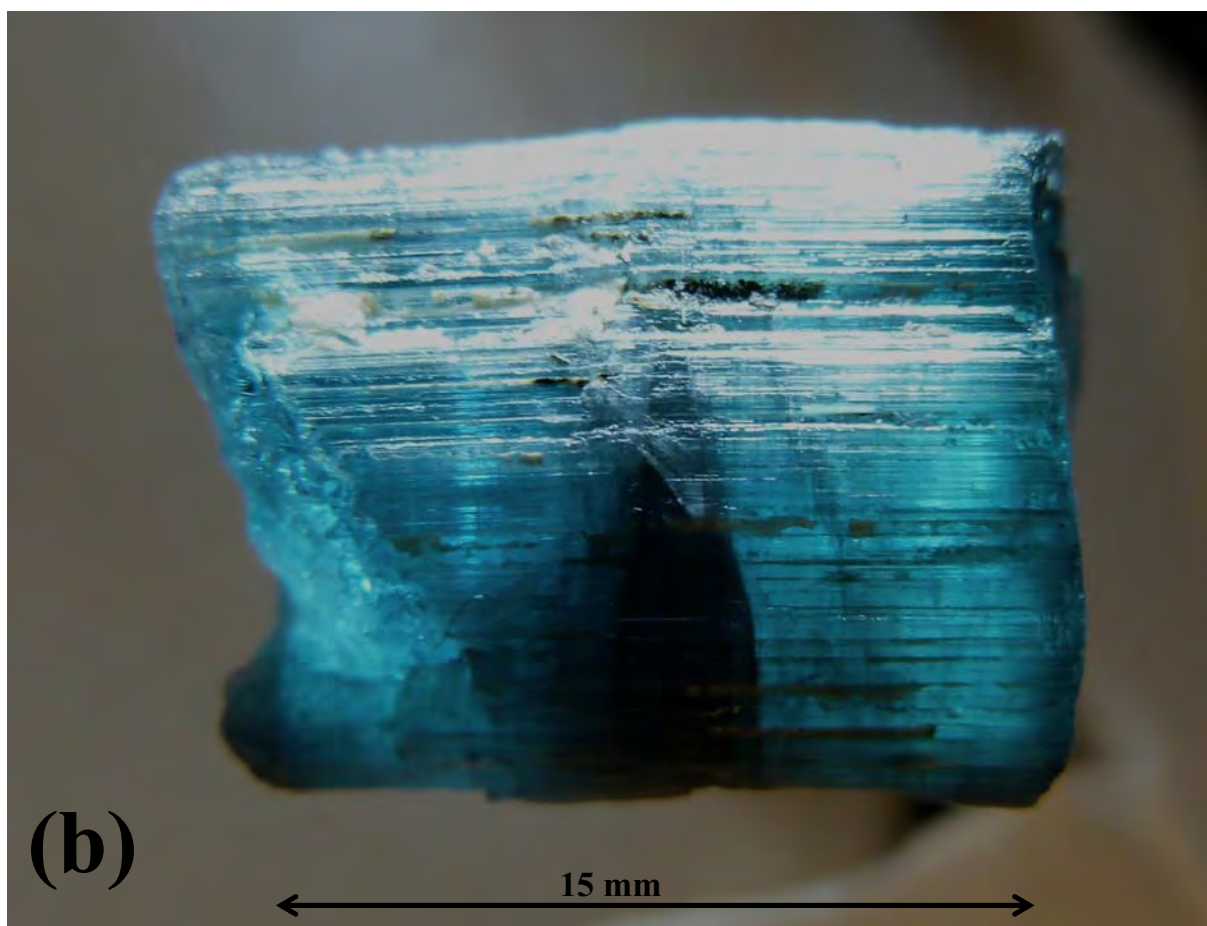


FIGURE 3

